Desalination and Water Treatment
www.deswater.com

doi: 10.5004/dwt.2023.30079

314 (2023) 88–102
December

Using banana waste biochar for simultaneous removal of heavy metals from raw real wastewater from the electroplating industry

Erasmo Arriola-Villaseñor[a], Alba N. Ardila A[a,*], Rolando Barrera Z[b], José Hernández[c]

[a]*Research Group in Environmental Catalysis and Renewable Energies, Facultad de Ciencias Básicas Sociales y Humanas, Politécnico Colombiano Jaime Isaza Cadavid, Apartado Aéreo 49-32, Medellín, Colombia, emails: anardila@elpoli.edu.co (A.N. Ardila A), erasmoarriola@elpoli.edu.co (E. Arriola-Villaseñor)*
[b]*CERES Research Group, Engineering Faculty, Chemical Engineering Department, Universidad de Antioquia, Calle 70 No. 52-21, Medellín, Colombia, email: rolando.barrera@udea.edu.co*
[c]*UPIIG, del Instituto Politécnico Nacional, Av. Mineral de Valenciana 200, Col. Fraccionamiento Industrial Puerto, 36275 Silao, Guanajuato, México, email: jahernandezma@ipn.mx*

Received 26 June 2023; Accepted 9 October 2023

ABSTRACT

The simultaneous removal of heavy metals (Fe^{2+}, Zn^{2+}, Ni^{+2}, Cr^{2+}, and Cu^{2+}) using filters built with cheap and easily accessible materials was studied in raw real wastewater generated from an electroplating industry localized in Medellín-Colombia. Various synthesized materials from banana peel waste were used as adsorbents, including powdered dry biomass and functionalized (chemically treated with activating agents) and unfunctionalized biochars, all obtained via hydrothermal and pyrolytic synthesis. For comparison, a commercial activated carbon (CAC) was employed. Significant variations in both structural and surface characteristics were observed among the materials depending on the activating agents utilized. As it was raw wastewater, the coexistence of multiple metals posed challenges in the objective comparison of adsorbents. Thus, the normalization of the maximum adsorption capacity about various parameters (for example, the amount of adsorbent, the specific surface area, the type and abundance of superficial functional groups, or the diameter and volume of the pore) confirmed the complexity of this type of process. In general terms, CAC and unfunctionalized biochar exhibited the highest adsorption capacities (for most metals). This suggests that, when employing banana waste adsorbents for the simultaneous removal of heavy metals in electroplating industry wastewater, the functionalization processes (which involve energy consumption, reagent usage, and waste generation) may not be necessary.

Keywords: Banana peels; Real wastewater; Electroplating industry; Heavy metals; Biochars; Activating agents

1. Introduction

Heavy metals such as Fe^{2+}, Zn^{2+}, Ni^{2+}, Cr^{2+}, and Cu^{2+} usually appear in wastewater generated from the electroplating industry, given their intensive use for surface coatings in the pickling stages [1,2]. Sometimes, the final deposition of these metals can cause environmental problems. According to data reported in the literature [3–9], significant amounts of these pollutants are discharged directly into water sources, affecting the pH of the water and generating negative impacts on flora, fauna, and human health [1,2]. Further, unlike most organic contaminants, heavy metals are not biodegradable and accumulate within living organisms, causing carcinogenic, mutagenic, and teratogenic effects [1,2]. Among the most common alternatives for effluents treatment and contaminants removal are adsorption methods

* Corresponding author.

using commercial activated carbon (CAC). This is a widely used material due to its porous structure, high surface area, chemical and thermal stability, and high adsorption capacity [10]. However, its major drawbacks include high production costs and its generation from fossil raw materials such as coal, petroleum tar, and phenolic resins [11]. In order to reduce the use of non-renewable sources, mitigate high costs, and adopt eco-friendly processes, various methodologies have been proposed for the synthesis of bioadsorbents obtained from various agro-industrial residues, in recent years [12].

In this context, Colombia offers great opportunities for agro-industrial production, given the fertile soils in its various regions and government efforts to promote environmental care, social development, and circular economy. Particularly, the banana industry (with significant production in various regions of the country), represents one of the industrial sectors showing high growth and development. Consequently, it results in greater generation of solid organic waste: once the bunch of edible fruit is detached from the stem to be marketed, the rest of the plant becomes a residue of quite pronounced volume. In addition, out of the total mass of the edible fruit, only between 20% and 30% is used and the rest is discarded [13,14]. Therefore, using this waste (both abundant and cheap) as an input to obtain bioadsorbents represents an interesting alternative.

The efficiency of the adsorption processes depends on several factors such as type, quantity, surface composition, and physico-chemical characteristics of the adsorbent; the chemical nature and concentration of the adsorbate; and the conditions of the adsorption process such as the pH of the medium, temperature and residence times [15–17]. According to the literature, physico-chemical properties (porosity, specific surface area, and surface functional groups) as well as the adsorption capacity of biochars from lignocellulosic waste can be improved by using various types of physical activation (size reduction by ball milling, radiation activation, microwave heating, plasma radiation, electrochemical heating, and ultrasonic agitation) or chemical activation (acids, alkalis, metal oxides, organic solvents, polymers, or exposure to an oxidizing medium such as steam, hydrogen peroxide, carbon dioxide, ozone, or air) [18–21]. Some studies have shown that physical activations improve the architectures of biochar mesopores and micropores [22], while the use of acids and bases allows an increase in adsorption sites, promoting electrostatic attraction, surface complexation, and surface precipitation [18–21]. Nonetheless, it has also been demonstrated that the use of activating agents does not always have a positive impact on the physico-chemical properties of the adsorbent or on its adsorption capacity [22,23].

Table 1 presents an overview of several studies focusing on the use of bioadsorbents derived from lignocellulosic waste modified with various chemical agents. Most of the studies used ideal solutions and a low fraction of them used synthetic industrial wastewater with a maximum of three contaminants. It is evident that none of them has used raw wastewater. Thus, according to the literature review, there is currently no available information regarding the experimental application of these adsorbents in real untreated wastewater. Consequently, the data regarding the practical utilization of adsorbents in real untreated wastewater (which contains multiple pollutants) are limited [24,25]. The incorporation of real untreated wastewater in adsorption investigations poses a significant challenge due to its intricate composition and the potential synergistic interactions among various pollutants [26]. Unlike most related studies in the literature, in this contribution bioadsorption process was carried out using real raw wastewater; therefore, the results are expected to help close technological gaps between research on bioadsorbents and their real industrial applications being that kind of investigation novel, crucial research to focus on the efforts towards investigating this topic by employing a real matrix under typical conditions of current industrial wastewater, due this approach can effectively contribute to the resolution of specific industry-related issues.

In the present investigation, adsorbent materials were synthesized from agro-industrial waste generated by the banana sector (banana peels), using different activating agents ($NaHCO_3$, $ZnCl_2$, and $FeSO_4{\cdot}7H_2O$). The adsorption process was carried out using a simple, low-cost homemade filter, in a continuous flow setup. The study aimed to elucidate the impact of chemical activation on the surface, morphological, and structural characteristics of the synthesized adsorbents, as well as their efficiency in removing various heavy metals from real raw wastewater. Moreover, the biochars were evaluated using simultaneous adsorption processes for Fe^{2+}, Zn^{2+}, Ni^{+2}, Cr^{2+} and Cu^{2+} present in raw wastewater generated by the electroplating industry; determining their maximum adsorption capacity; and comparing it with CAC as a reference adsorbent. Furthermore, to discern the effect of each chemical agent in the adsorption processes of various metals, a normalization of the maximum adsorption capacity was conducted concerning several parameters, including the quantity of adsorbent, specific surface area, surface functional group type and abundance, pore diameter, and pore volume.

2. Materials and methods

2.1. Obtention and physico-chemical characterization of biochars

For the synthesis of the biochars, banana peels of the Gros Michel variety were used. These had been classified as rejection bananas, which did not meet the quality standards for commercialization (NTC 1190, Banana) [39]. This raw material was supplied by the ASOFRUCOL Trade Association located in Itagüí-Colombia. The waste fruit was pulped; the peels were washed with deionized water to remove impurities; they were cut with sizes of approximately 2 cm and dried for 72 h at 80°C in a convection oven; and finally ground in a mill and coded as USB.

Unfunctionalized biochar (UBSB) was obtained from USB biomass by pyrolysis in an N_2 atmosphere, within a batch system at 5°C/min up to 600°C for 3 h. For the synthesis of biochars functionalized using various activating agents, approximately 22.5 g of solid powdered biomass (USB) was weighed and mixed with 225 mL of deionized water and left under magnetic stirring (250 rpm) for approximately 3 h at room temperature. Subsequently, the mixture was transferred to a Teflon glass, which was deposited in a stainless-steel autoclave, taken to a convection oven

Table 1
Comparison of the adsorption capacity and removal percentage for various pollutants using bioadsorbents derived from different biomass sources

Biomass source	Active agent	Metal	Hue type	Adsorption conditions	Removal (%)	Adsorption capacity (mg/g)	References
Tectona grandis tree sawdust	Biochar-K_2CO_3 Biochar-$ZnCl_2$ Biochar	Cr^{6+}	Aqueous solution	5–200 mg/L of Cr, 150 rpm, 24 h, 30°C and 50 mL of solution, pH = 3.0	– – –	103 127 83.5	[27]
		Cu^{2+}			60.93	0.00364	
Corn straw	KOH	Cr^{6+}	Aqueous solution	Contact time (0–600 min), pH = (1, 3, 5, 7, and 9), adsorbent dose for 100 mg/L, 180 rpm, 16 h	98.32%	175.44	[28]
Fox nutshell	$ZnCl_2$	Cr^{6+}	Aqueous solution	10 mg/L, 250 mL 150 rpm, 30°C, 3 h, 0.05g adsorbent	99.08%	43.45	[29]
Apple peels	Phosphoric acid (H_3PO_4 85%)	Cr^{6+}	Aqueous solution	10–50 mg/L Cr(VI), pH (2–7), and temperature (10°C–40°C), time of 2 h, 400 rpm, (0.025–0.15 g/50 mL) adsorbent	95%	36.01	[30]
Commercial materials	H_2SO_4/HNO_3 (180:20 mL)	Cr^{6+}	Aqueous solution	20 mg/L Cr^{6+}, pH (2.5 to 4.0), 40 min, 150 rpm, 0.5 g adsorbent	–	85.83	[31]
Waste tires (TAC) and from the pyrolysis of sawdust (SPC)	Actives with CO_2	Cr^{6+}	Aqueous solution	60 mg/L, 200 mL, 2 h, pH = 2, 150 rpm, 22°C, 0.4 g adsorbent	99%	29.93	[32]
Banana peels	H_3PO_4	Mn^{3+}, Fe^{2+}	Aqueous solution	25 mL of 10 mg/L, pH = 7.0 at 150 rpm and 25°C, 3 h	Mn: 46% Fe: 96%	Mn: 3.03 Fe: 32.99	[33]
Banana peel-alkali (BBP) Eucalyptus bark alkali (BEB)	NaOH	Pb^{+2}, Ni^{+2}	Aqueous solution	500 mg/L (Ni^{2+}:Cd^{2+}) 1 h, pH = 5.0, 20°C 70 rpm, 0.1 g adsorbent	BBP: 97.0% (Pb^{2+}) 50.7% (Ni^{2+})	BBP: 65.9 (Pb^{2+}) 17.1 (Ni^{2+}) BEB: 39.6 (Pb^{2+}) 8.99 (Ni^{2+})	[34]
Banana peels	$FeSO_4{\cdot}7H_2O$ and $FeCl_3{\cdot}6H_2O$	Cu^{2+}, Hg^{2+}, Zn^{2+}	Aqueous solution	50–250 mg/L, 250 mL, pH = 6, 150 rpm, (10–360 min), room temperature, adsorbent (0.2–1.0 g/L)	76%–85%	72.8 (Zn^{2+}), 75.9 (Cu^{2+}), and 83.4 (Hg^{2+})	[35]
Banana peel	Fe_3O_4 (BPB/Fe_3O_4/ZIF-67$_{nanoparticles}$)	Cd^{2+}	Aqueous solution	10 mg/L, 40 min, pH = 6, 30°C, adsorbent 1 g/L	99.14%	50.78	[36]
Banana peel (magnetic nanocomposites)	Fe_3O_4	Cu^{2+}	Aqueous solution	10 mg/L, 90 min, pH = 6, 40°C, 1 g/L adsorbent	99.46%	73.23	[37]
Corncobs	$Na_2S_2O_3$	Pb^{2+}, Cu^{2+}	Aqueous solution	1,000 mg/L, 4 h, 25°C, 180 rpm, 250 mL, 0.1 g biochar	Cu^{2+}: 40% Pb^{2+}: 55%	421.8 (Pb^{2+}) 188.0 (Cu^{2+})	[21]
Banana peels FBPB fresh banana peel DBPB dehydrated banana peel	H_3PO_4	Cr^{6+}, Pb^{+2}	Aqueous solution	200 mg/L, 40 mL, 3 h, pH = 4, room temperature, 150 rpm, 0.01 g biochar	72.05% FBPB 73.35% DBPB	359 DBPB 193 FBPB	[38]

preheated to 190°C, and left for 6 h to produce the hydrochar. Following the hydrothermal synthesis process, the hydrochar was filtered and washed with 100 mL of a water-ethanol mixture (3:1) and dried at 105°C for approximately 6 h. Subsequently, a certain amount of dry hydrochar (previously macerated) was weighed and mixed with the necessary amount of activating agent: $NaHCO_3$, $ZnCl_2$, and $FeSO_4 \cdot 7H_2O$, to obtain an impregnation ratio of 0.75:1, 1.75:1, and 0.27:1 of reagent activator/hydrochar for BSBF-Na, BSBF-Zn, and BSBF-Fe, respectively. Subsequently, deionized water was added as a solvent (30 mL per approximately 8 g of hydrochar). Next, each solid was dried from the previous mixture at 105°C for 24 h, and then pyrolyzed under the same conditions described above. Once each material was pyrolyzed, the biochar was washed first using 0.1 M HCl if necessary and then with deionized water, until a pH value of 7.0 was obtained in the filtrate. Finally, the solids were dried at 105°C until a moisture content of less than 5% was obtained. They were then stored in a dark hermetic container before use. All the materials were sieved through an ASTM 40 mesh to obtain a fine material with a homogeneous particle size (diameter < 0.42 mm). In addition, throughout the synthesis process, corresponding weighing was carried out to calculate the yields for each material obtained. The CAC used was DARCO 20-40 type and produced by Norit (Norit Americas Inc.).

The dry powdered biomass, the various functionalized biochars, and the CAC were characterized by X-ray diffraction using a Bruker diffractometer (D-8) having a Cu Kα radiation source, an Ni filter at 40 kV and 40 mA, and a wavelength equal to 1.54 Å. The diffraction intensity as a function of the angle 2θ was measured between 15° and 70° 2θ using the step rate of 0.02°/min 2θ. The textural properties were determined using equipment of the Micromeritics Brand (ASAP 2020), through N_2 adsorption–desorption isotherms of the bioadsorbent at 75.2 K. The Brunauer–Emmett–Teller equation was used for determining the surface area based on N_2 isotherms. Fourier-transform infrared spectra with attenuated total reflectance (FTIR) were obtained using a Shimadzu IR spectrophotometer (IRAffinity-1S) in the range of 400–4,000 cm^{-1}. The morphology of the biochars were investigated by using a field emission scanning electron microscopy (SEM) in a JEOL JSM 5800 at 5.0 kV. The isoelectric point or point of zero charge (pzc) of the biomasses was determined by mass titration, which involved finding the asymptotic value of the pH of a bioadsorbent/water suspension as its mass content increased. To obtain the pH values, a ratio of biochar/water of 20, 40, 60, 80 and 100 mg by weight was used; the resulting pH values were measured after 24 h of equilibration. Finally, the concentrations of phenolic, carboxylic, and lactonic surface groups were determined through the Boehm Method, using potentiometric titrations with 0.05 M standardized solutions of NaOH, Na_2CO_2, $NaHCO_3$ and HI-8424N Hanna Instruments pH Meter.

2.2. Filter construction

For the construction of the filter, recommendations from the literature were followed [40,41]. A homemade tubular multilayer filter was used (Fig. 1) with 1" polyvinyl chloride pipe and fittings. Fine silica sand and coarse sand from crushed volcanic material were used as filtering media. These materials were sieved to obtain a uniformity factor < 1.3; this ensured sufficiently homogeneous material and reduced backwash requirements. Both the sand and the gravel were manually washed 12 times with tap water until colorless decanted water was obtained. Subsequently, the materials were dried in a convection oven at 105°C for 12 h and stored in hermetic containers.

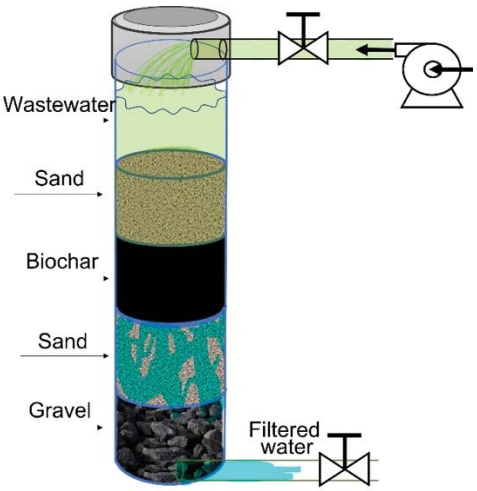

Fig. 1. Diagram of the filtration system manufactured for adsorption processes.

A filter in continuous operation was used, since it could represent application in wastewater generated from the electroplating industry to a greater extent. Also, it could provide practical information about the adsorption capacity, regarding operating parameters such as flow rate, residence time, and volume of the adsorbent. To ensure the flow of the filtered liquid, an adjustable peristaltic pump was used within a slow or biological filtration regime (0.08–0.6 $m^3/m^2 \cdot h$), in this case ≈ 0.03 $m^3/m^2 \cdot h$. This is favorable for the implementation of processes that do not require complex infrastructure or considerable energy investment. The multilayer filter (sand-adsorbent-sand-gravel) was built using 5 cm per layer and 1.25 cm internal diameter [11]. The operating parameters are summarized in Table 2 and are set according to literature reports at laboratory scale and pilot scale [11,28].

2.3. Sampling and physico-chemical characterization of real raw wastewater from electroplating industry

The electroplating industry effluent was obtained from a company located in the city of Medellín. A gauging day and a sampling plan were implemented to obtain a representative composite sample of the effluent. The sampling session consisted of taking a sample volume of 2 L of raw raw real wastewater (RRW), every half hour for 6 h, at the outlet of a homogenization tank storing discharges from different processes. Simultaneously, physico-chemical parameters were measured in situ: temperature, pH, color, turbidity, and conductivity. *Ex-situ* parameters, such as chemical oxygen demand (COD), biochemical oxygen demand (BOD_5), total

organic carbon (TOC), and heavy metals and interest were analyzed. All the samplings and physico-chemical characterization were carried out following the Standard Methods of Examination of Surface Waters and Wastewater (Table 3). The target metals were analyzed before and after the adsorption process on the real RRW using an atomic absorption spectrophotometer with an air-acetylene-nitrous oxide flame, Agilent 240FS. Initially, the performance parameters of the equipment were optimized for the determination of each metal. Once these conditions were established, 6 standards were prepared, with each containing the 5 metals (Fe, Cu, Ni, Zn and Cr), in order to obtain the calibration curves.

2.4. Filter adsorption tests using raw industrial wastewater

The adsorption system was uniformly tested using various adsorbent materials. First, control tests were carried out only using sand, and without using the filtering material or CAC. The filtering process was carried out for 6 h, and samples of 15 mL were taken every 8 mL throughout the process.

Table 2
Constructed filter operating parameters

Parameter	Value
Cross-sectional area (cm^2)	≈5.0
Linear speed (cm/min)	0.42
Mass flow or flow rate (mL/min)	≈2.1
Adsorbent volume (cm^3)	50.2
Residence time (min)	≈10.0
Biochar volume normalized flow ($mL_{sln}/(min \cdot cm^3_{ads})$)	≈0.1

The removal percentage of each metal was evaluated using atomic absorption spectrophotometry and calculated using Eq. (1).

$$\text{Removal}(\%) = \frac{C_0 - C_f}{C_0} \times 100\% \quad (1)$$

where C_0 and C_f are the concentration of each metal before and after the adsorption process, respectively.

The adsorption capacity in terms of contaminant retained per gram of adsorbent material (adsorption capacity q_b) was determined, in units of mg/g_{ads}, using Eq. (2).

$$q_b = \frac{Q_v \cdot t_{10\%} \cdot C_0}{m \cdot 1000} \quad (2)$$

where q_b = adsorption capacity (mg of adsorbate per gram of adsorbent), Q_v = volumetric flow rate (mL/min), $t_{10\%}$ time (min) when the column outlet concentration is 10% of the concentration at filter inlet (C_0), C_0 = initial concentration (mg/L), and m = mass of adsorbent (g).

3. Results and discussion

3.1. Physico-chemical characterization of raw real wastewater

Table 3 describes the results of the physico-chemical characterization of RRW. The values obtained for COD, pH, and total suspended solids are lower than those reported in the literature for wastewater of the same nature [26]. However, these values exceed the maximum permissible limit (MPL) established in Colombian Regulations. Parameters such as conductivity, turbidity, color, total solids, and total dissolved solids are not contemplated in Colombian Regulations to be controlled in this type of effluent, and their values are significantly lower than those reported in the literature

Table 3
Physico-chemical parameters evaluated and applied method

Parameter/Unit	Method	Value	TLV[a] [43]
pH (U of pH)	AWWA-4500H+	3.65	6–9
Temperature (°C)	AWWA-4500H+	22.5	–
Electrical conductivity (μS/cm)	AWWA-2510B	20.1	–
Turbidity (UNT)	AWWA-2130B	97.3	–
Colour (UPC)	AWWA-2120	500	–
Total solids (mg/L)	AWWA-2540B	1180	–
Total suspended solids (mg/L)	AWWA-2540E	122.22	50
Total dissolved solids (mg/L)	AWWA-2540C	955	–
Chemical oxygen demand ($mg \cdot O_2/L$)	AWWA-4500C	360	250
Biochemical oxygen demand (BOD_5) ($mg \cdot O_2/L$)	AWWA-5210B	10.6	100
Total organic carbon (TOC) (mg/L)	AWWA-5310B	94.6	–
Total zinc (mg·Zn/L)	AWWA-3500 Zn B	18.7	3.00
Total nickel (mg·Ni/L)	AWWA-3500 Ni B	10.1	0.50
Total iron (mg·Fe/L)	AWWA-3500 Fe B	11.2	3.00
Total copper (mg·Cu/L)	AWWA-3500 Cu B	36.7	1.00
Total chromium (mg·Cr/L)	AWWA-3500 Cr B	0.44	0.5

[a]Threshold limit values.

for other similar effluents [22,42]. The value obtained for the COD exceeds the MPL established in the Colombian Regulations, while the BOD_5 is below the MPL. However, the values for both parameters are much lower than those reported in the bibliography for this type of wastewater. No data regarding TOC was found in the consulted literature. Further, this parameter has not been contemplated in the existing Colombian Regulations.

The calculated biodegradability index (taken as the BOD_5/COD ratio) was 0.029, which chiefly indicates the presence of inorganic matter that is difficult to biodegrade, in this case, mainly heavy metal salts. On the contrary, the high value obtained for the COD/TOC ratio (3.80) indicates a low content of organic compounds of a biodegradable nature. Additionally, the concentration analyzed for various heavy metals identified (Zn, Ni, Fe, Cu, except Cr) exceeds the maximum permissible limits established in the existing Colombian Regulations.

3.2. Physico-chemical characterization of biochars

Table 4 presents the results of the characterization, corresponding to some physico-chemical parameters for the different materials evaluated, including CAC used as a reference. The yield for obtaining powdered dry biomass was 78%, while for biochar it ranged between 30% and 50%, which agrees with reports in the literature [44]. The different yield percentages show that the highest yield of 52.2%, higher than the non-functionalized material UBSB (38.1%) was achieved with the functionalized material BSBF-Na. This finding is similar to various studies [45] reporting that the high percentages of yield in obtaining biochars may be related to the stabilization of carbon in the biochar, as a result of additives added prior to the pyrolysis process. However, the yield for the materials BSBF-Fe and BSBF-Zn (31.7% and 29.6%, respectively) was lower than the unfunctionalized material.

Fig. 2 shows the X-ray diffractograms of various materials, wherein the USB biomass mainly shows a wide peak of low intensity, with a center at an angle 2θ of 21.5° and an almost imperceptible peak at an angle 2θ of 24°, characteristic of slightly crystalline materials of cellulosic nature [46] made up of hemicellulose and lignin [47]. However, post pyrolysis, this peak disappears in the UBSB, BSBF-Na, BSBF-Zn, and BSBF-Fe materials, due to the decomposition of the biomass material [48]. In the UBSB biochar diffractogram, a predominant intense peak is observed at 2θ = 28.37° associated with the turbostatic structure of carbon graphite [47]. The other additional peaks are related to thermally decomposed fullerene and kaolite. Thus, the peaks at 2θ = 30.3°, 31.4°, 37.8° and 40.58° are attributed to kaolite, while the peaks at 2θ = 11.4° and 31.7° correspond to fullerenes [47]. The Na-modified material shows lower crystallinity, thus yielding a mostly amorphous material, which may be related to the coordination of Na ions that do not allow the formation of crystalline structures in the biochar [46].

CAC presents a diffractogram characteristic of this type of material, with a broad band in 2θ between 20° and 30° assigned to highly disordered graphite carbon [49], with a pronounced peak at 27° corresponding to the 002 plane of graphite [48], as well as a small peak at 21° related to quartz impurities in these materials [50]. The small broad peak centered around 42° corresponds to the 100 plane and indicates small domains of ordered graphene sheets [36,47,51]. As in the CAC, most materials present a broad peak centered around 24°, which corresponds to the 002 plane of the graphite microcrystals in each biochar [52].

Fig. 3 shows the adsorption–desorption isotherms of each material. Here, it can be seen that, according to the International Union of Pure and Applied Chemistry (IUPAC) classification, the adsorption isotherms of all biochars are type II and III, with laminar-shaped pores [53,54] of the order of mesopores (2–50 nm). This is consistent with the results obtained in relation to the pore diameter (Table 4). Specifically, the USB and BSBF-Zn materials showed the type II isotherm without hysteresis, characteristic of non-porous solids or macroporous adsorbents. This proved that these two biochars correspond to non-porous materials since the reported pore diameters do not meet the characteristics of macropores (>50 nm). Further, although the reported values of pore diameters are characteristic of mesoporosity, these two materials presented the lowest value with respect to pore volume: 0.0055 and 0.00055 cm^3/g, respectively, which supports low or almost zero specific surface area. Regarding the type of hysteresis, according to the IUPAC classification (H1-H5), and its relationship with the specific structure of the pores, it was observed that the BSBF-Na and BSBF-Fe materials present H3 type hysteresis, associated with aggregates of particles with sheet-shaped pores. In case of the UBSB and CAC materials, there exists an H4 type hysteresis,

Table 4
Physico-chemical properties of biochars

Characteristic	USB	UBSB	BSBF-Na	BSBF-Zn	BSBF-Fe	CAC
Global yield (% wt.)	78.24 ± 0.68	38.14 ± 0.28	52.20 ± 0.68	29.61 ± 0.54	31.74 ± 1.58	–
Specific surface area (m^2/g)	2.3	154	56	0.34	378	650
Average pore volume (cm^3/g)	0.0055	0.0198	0.063	0.00045	0.291	0.94
Average diameter volume (nm)	5.43	33.82	5.24	5.34	3.09	41.10
Isoelectric point	6.40	7.42	6.69	6.48	7.20	7.20
Carboxylic surface groups (μmol/g)	5.5	10.1	0	3,438	0	7.2
Lactonic surface groups (μmol/g)	453.1	3,375	0	189	0	0
Phenolic surface groups (μmol/g)	656.3	9,625	0	629	2,399	359.1
Total surface groups (μmol/g)	1,114.9	13,010.1	0	4,256	2,399	366.3

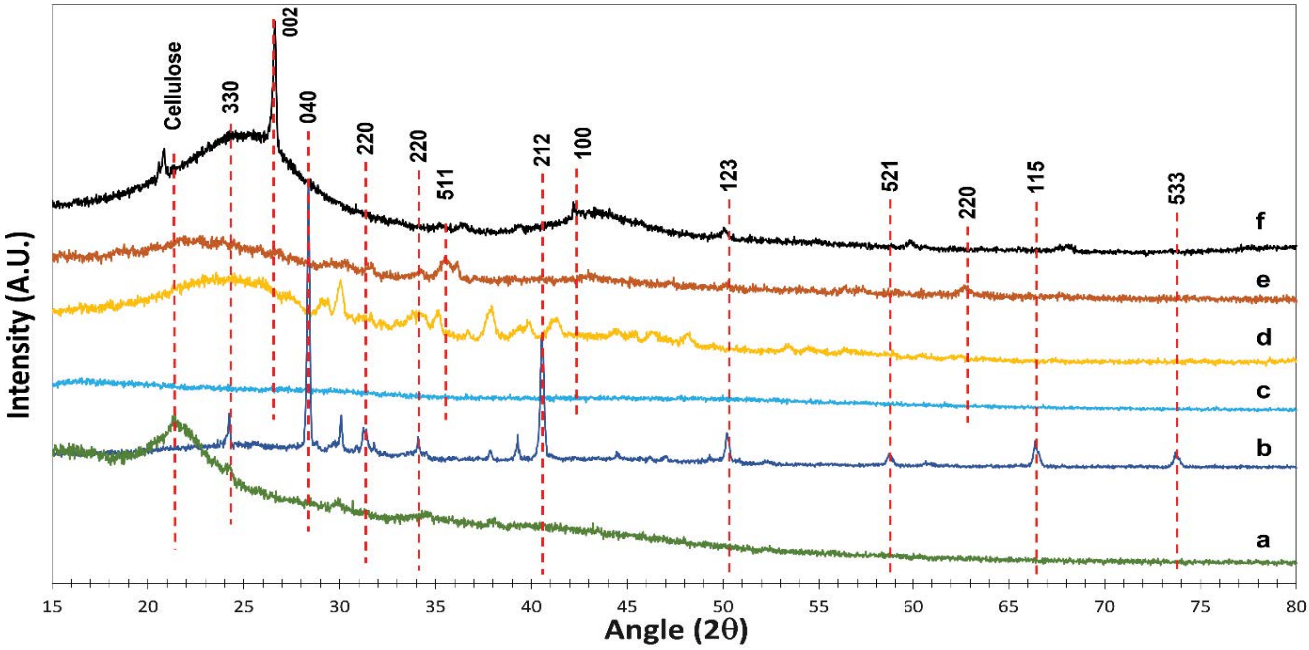

Fig. 2. X-ray diffraction patterns of bioadsorbents: (a) USB, (b) UBSB, (c) BSBF-Zn, (d) BSBF-Na, (e) BSBF-Fe and (f) CAC.

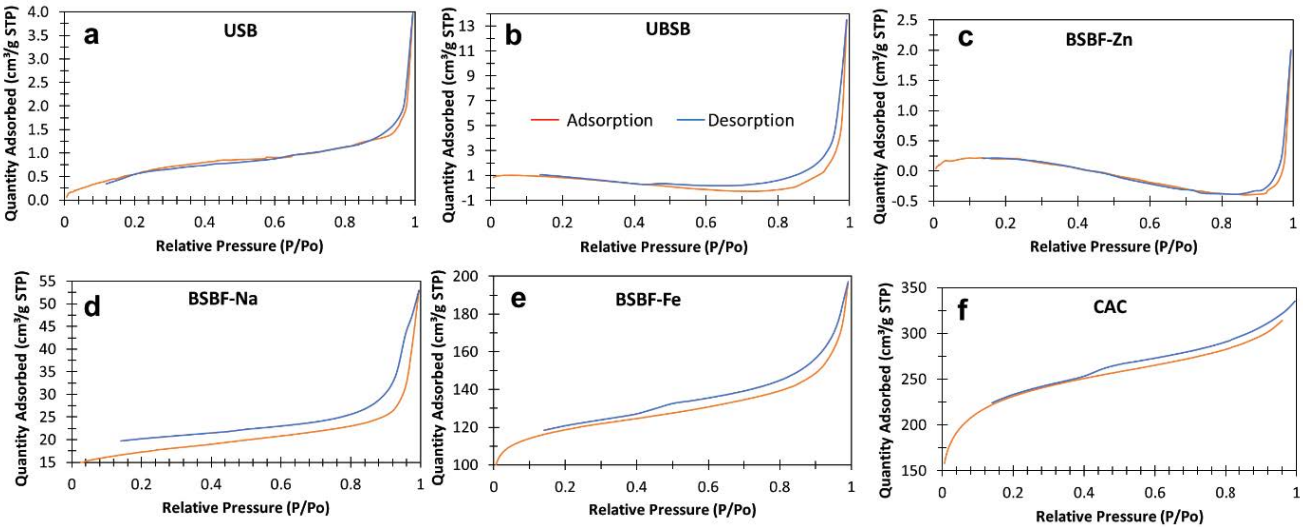

Fig. 3. Adsorption–desorption isotherms of different biochars: (a) USB, (b) UBSB, (c) BSBF-Zn, (d) BSBF-Na, (e) BSBF-Fe and (f) CAC.

closing the hysteresis loop at a relative pressure of 0.5, which indicates very narrow sheet-shaped pores, as well as the presence of additional micropores [54].

Other biochar characteristics commonly affected due to the use of activating agents are porosity, surface area, pore size, and volume, among others. In relation to the specific surface area, the dry powder biomass showed a minimum value of 2.3 m^2/g. This is consistent with reports in the literature where significantly low values (<5 m^2/g) have been obtained for biomasses from agro-industrial residues [55,56]. However, it is important to note that other reports list significantly higher values (for example, 154 m^2/g) for another class of biomasses, indicating that this parameter is closely related to the type of raw material used [52]. In relation to the surface area of the biochars, the results obtained in this study show that the material activated with Fe (BSBF-Fe) presented an increase in the value of the specific surface area, slightly more than double compared to the material without functionalization. On the other hand, in the materials chemically activated with Na and Zn (BSBF-Na and BSBF-Zn), the opposite effect occurred, the area obtained was 56 and 0.34 m^2/g, respectively, values significantly lower than that of the UBSB material without functionalization (154 m^2/g). According to some studies, different values are found in parameters such as surface area and porosity of similar materials, but they are synthesized under different conditions

in terms of pyrolysis temperature, nature of the biomass, and/or biomass/activating agent ratio [23].

The Boehm analyzes are listed in Table 4, there is a significant modification in terms of the surface composition (carboxylic, lactone, and phenolic acid functional groups) of the materials synthesized using different activating agents. For example, in biochar BSBS, a significant increase in the abundance of the three superficial functional groups is observed in comparison with the dry powder biomass (USB), which is much higher even than that obtained for the CAC used as reference material [57]. Numerous investigations have shown that pyrolysis increases the abundance of oxygenated surface groups in the biomass derived from aromaticity [45,58].

As for the adsorbent BSBF-Na, treatment with Na caused a drastic decrease in all acid surface groups (carboxylic, lactonic, and phenolic). According to the literature [34], the use of alkalis in obtaining biochars favors the presence of basic active sites on the surface of the material, thus reducing acid surface groups. This behavior may be due to the neutralization or protonation of carboxylic groups and the subsequent formation of carboxylate groups. These results are consistent with the FTIR spectra, wherein it is observed that the bands around 1,150; 1,250 and 1,400 cm^{-1} associated with C–O, C–O–C, and C=O bonds, respectively of carboxylic groups disappear entirely in the material. Similar results were obtained from other investigations, stating that this phenomenon is caused by a decarboxylation process promoted by the alkaline hydrolysis of lignin and hemicellulose [34].

Although in all biochars synthesized using various activating agents, the phenolic and lactonic groups decrease significantly compared to those of the unfunctionalized biochar, it is observed that the presence of Zn increases the carboxylic groups. Thus, the BSBF-Zn material contains a greater quantity of these functional groups, even greater than the CAC, wherein such superficial functional groups are not identified. The results of the Bohem method are coherent and agree with those obtained by the FTIR technique (Fig. 4). Fig. 4 shows that the bands associated with the lactonic, and phenolic functional groups decreased considerably while modifying materials using various activating agents, being more evident for the UBSB-Na and UBSB-Fe materials. Thus, it was observed that the bands related to different bond stretching vibrations associated with stronger acid groups such as carboxylic ones decreased in intensity or even disappeared. For example, the bands with bond vibrations at 1,080 cm^{-1} (C–O) [59], 1,515 cm^{-1} (C=C) [34,35], showed a decrease in intensity or disappearance in the BSBF-Na materials, BSBF-Zn, and BSBF-Fe, compared to UBSB and CAC bioadsorbents. On the other hand, the bands at 1,730 cm^{-1} associated with bonds (C=O) of carboxylic groups [34] and 2,300 cm^{-1} (C=C) [35,38] remained relatively constant. A similar phenomenon occurs with the band centered at 1,400 cm^{-1}, associated with the vibration of O–H bonds of the phenolic groups [35] since this band is not observed for the BSBF-Na, BSBF-Fe, and CAC materials. Additionally, the bands centered around 2,900 cm^{-1} associated with sp_3 hybridization C–H bonds [52] and 880 cm^{-1} associated with the C–H aromatic bond, and the existence of π electrons [35], are seen to be lower in BSBF-Na, BSBF-Fe, and CAC, compared to the UBSB and BSBF-Zn materials. This decrease is associated with the loss of available aliphatic groups. However, the modification of the said band does not show a relationship with the adsorption capacities. Therefore, it is evident that the presence of these species does not affect the adsorption processes. Thus, it is deduced that the adsorption processes are probably not carried out through the interaction of π–π bonds. On the other hand, the band at 2,980 cm^{-1} corresponding to O–H characteristic

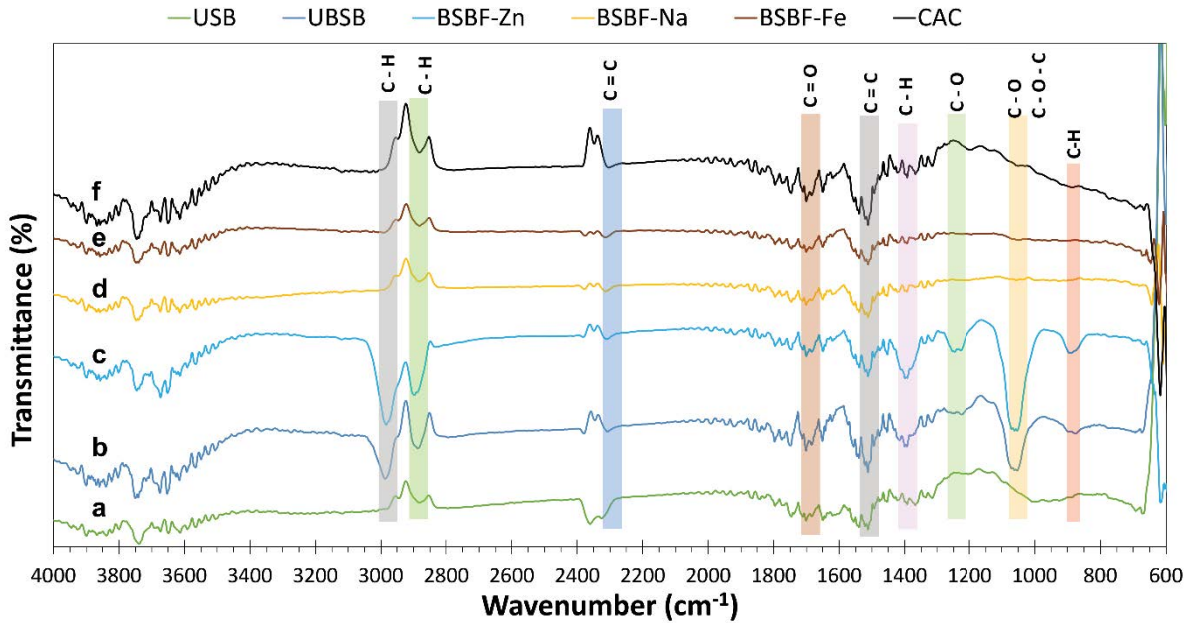

Fig. 4. Fourier-transform infrared spectrum of different biochars: (a) USB, (b) UBSB, (c) BSBF-Zn, (d) BSBF-Na, (e) BSBF-Fe and (f) CAC.

of hydroxyl groups [57] and the band at 1,228 cm^{-1} of the C–O carboxylate bond [35], generally associated with weak negative charges, appear only in UBSB and BSBF-Zn materials. This also implies the presence of these sites; however, a direct relationship with the adsorption results is not observed either.

The morphological properties of the synthesized materials were analyzed using SEM. Fig. 5 shows variations in

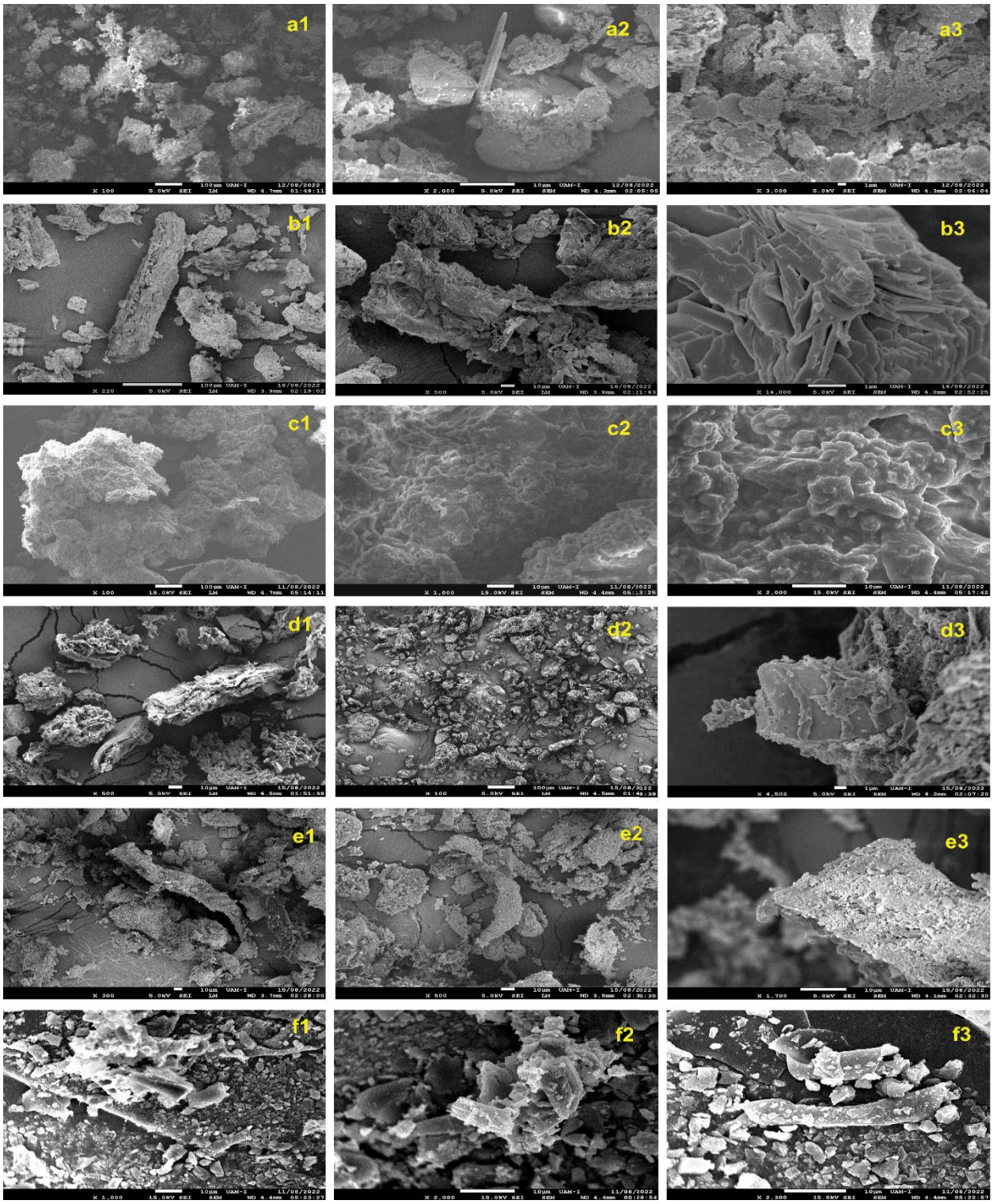

Fig. 5. Scanning electron microscopy images: (a1–a3) USB, (b1–b3) UBSB, (c1–c3) BSBF-Zn, (d1–d3) BSBF-Na, (e1–e3) BSBF-Fe and (f1–f3) CAC.

the morphologies and particle sizes among the obtained materials. For example, it can be seen that the BSBF-Na sample (Fig. 5d1–d3) has a rough surface morphology with little or no porosity, which is consistent with the results obtained. On the contrary, the UBSB biochar (Fig. 5b1–b3) exhibits a relatively smooth and compact appearance. Again, the BSBF-Fe material (Fig. 5e1–e3) exhibits a more rough and porous structure; this can be due to the reaction of Fe and iron oxides with the cellulose in the biomass, which, while releasing gas, produces a more spongy material and therefore, a greater surface area.

3.3. Adsorption tests

Fig. 6 shows the profiles of the removal percentages for each metal following evaluation after using various adsorbents. In the case of Cr (Fig. 6a), the best results were obtained with the UBSB and CAC materials, which presented a similar adsorption capacity. Additionally, in both materials, no significant changes were observed in the percentages of removal of this metal under the continuous operation of the filter for 6 h, thus maintaining a 100% removal in both cases. On the other hand, although the USB and BSBF-Fe adsorbents showed significantly high removal percentages (90%–100%) during the first 2 h of operation, they reached almost complete saturation in around 6 h. The remaining materials (BSBF-Zn and BSBF-Na) did not reflect the capacity for the adsorption of this metal, since they quickly saturated in around 40 min.

Regarding Fe, the UBSB, CAC, BSBF-Na, and BSBF-Fe adsorbents reflected removal percentages of 100%; however, after 5 h, a gradual saturation process begins to be observed for the first two materials, while for the last two, this phenomenon occurs rapidly after 2 h. The remaining materials (BSBF-Zn and USB) did not show the capacity for Fe adsorption, since almost complete saturation of the material was observed after around 40 min.

Additionally, for Ni and Zn contaminants, it is generally observed that the best adsorbent is CAC, with which a high percentage of removal (~100%) is maintained, whereas the other materials show very low or no adsorption capacity. Finally, for Cu, high removal percentages were not observed with most of the materials during the time evaluated. Although the CAC, UBSB, and BSBF-Na adsorbents showed removals between 90% and 100%, these values were maintained only during the first 80 min, with removal percentages falling between 10%–20% at 5 h. Only the BSBF-Fe material maintained a removal close to 80% until 5 h, falling to a value of 30% 1 h later, while for the USB and BSBF-Zn materials, the removal percentages were less than 40% after the first operating hour.

Table 5 lists the metals in decreasing order, concerning their maximum adsorption capacity obtained with each evaluated material. The results confirm that one type of adsorbent under certain adsorption conditions can have a high capacity for the simultaneous removal of one or more

Table 5
Descending order of maximum adsorption capacity for each heavy metal evaluated

Material	mg·metal/g·adsorbent
USB	$Cu^{2+} > Zn^{2+} > Ni^{2+} > Fe^{2+} > Cr^{3+}$
UBSB	$Fe^{2+} > Cu^{2+} > Zn^{2+} > Ni^{2+} > Cr^{3+}$
BSBF-Na	$Cu^{2+} > Fe^{2+} > Ni^{2+} > Cr^{3+} \approx Zn^{2+}$
BSBF-Zn	$Cu^{2+} > Fe^{2+} > Cr^{3+} > Ni^{2+} \approx Zn^{2+}$
BSBF-Fe	$Fe^{2+} > Cu^{2+} > Zn^{2+} > Ni^{2+} > Cr^{3+}$
CAC	$Zn^{2+} > Fe^{2+} > Cu^{2+} > Ni^{2+} > Cr^{3+}$

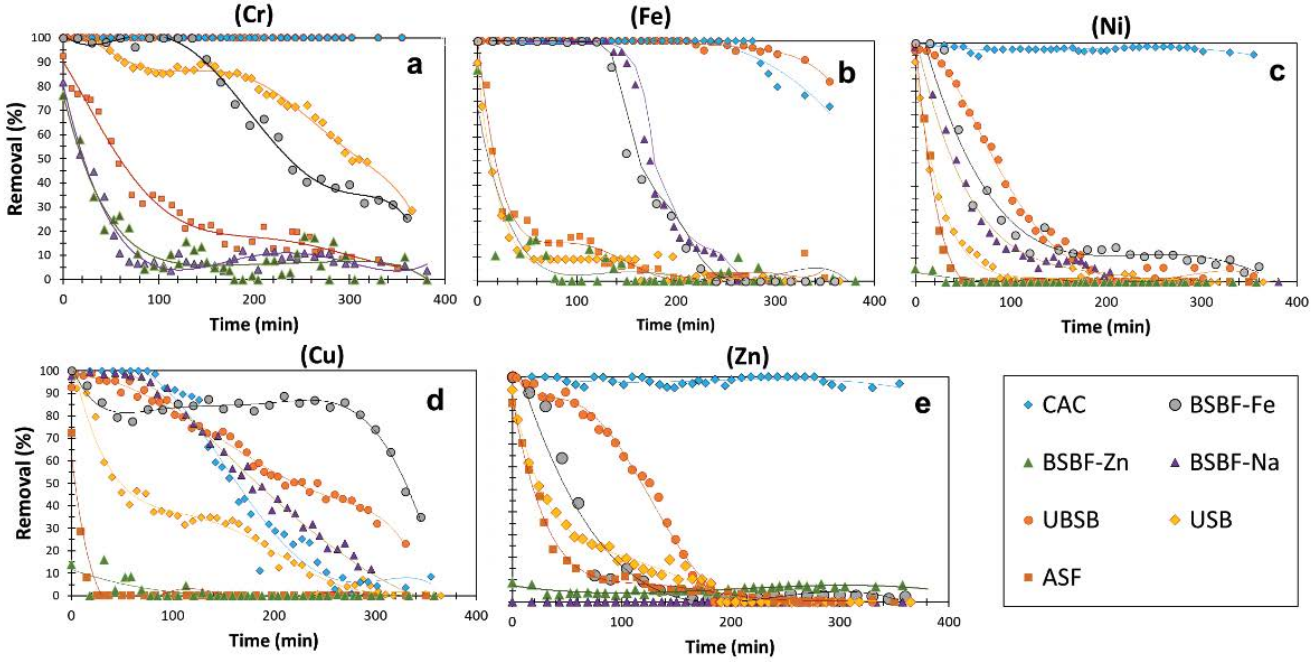

Fig. 6. Profiles of removal percentages of the different metals with each material.

heavy metals, while for others it does not. This indicates that the adsorption capacity depends on the physico-chemical nature of both the adsorbent and the contaminant as well as the type of interactions that can occur between them. Thus, this study cannot affirm that there exists an ideal adsorbent for the complete removal of all heavy metals found in the real wastewater analyzed. This demonstrates the importance of evaluating the effectiveness of an adsorbent in wastewater with a real composition. This is because varied competition and inhibition phenomena can occur among contaminants at different active sites, which can affect the efficiency of the adsorbents regarding each specific pollutant.

To identify the predominant characteristics of each material that could influence the adsorption processes of various metals, a normalization of the maximum adsorption capacity was carried out. This normalization was performed in relation to various parameters, such as the amount of adsorbent, specific surface area, type and abundance of surface functional groups, pore diameter, and volume. As can be seen in Table 6, the materials with the highest adsorption capacity in mg·metal/g·ads for most metals were CAC and UBSB. These results clearly show that the presence of the activating agents used in the present study did not improve the adsorption efficiency of most of the materials, since the highest adsorption capacities were achieved with the CAC and UBSB materials, both without any chemical agent. Further, the values obtained for these two materials are very similar or are in the same order of magnitude, indicating that the adsorbent that showed the best adsorption capacity in mg·metal/g·ads of the synthesized materials was UBSB (non-functionalized). This is interesting, since it suggests that it is unnecessary to carry out additional chemical activation processes: implying energy expenditure, use of reagents or activating agents, and generation of residues, to synthesize a potentially applicable material for the simultaneous removal of heavy metals from real wastewater generated by the electroplating industry.

Numerous studies have reported that the adsorption capacity of materials obtained from lignocellulosic raw materials can be increased with activations and chemical treatments [34]. However, it is also clear that all chemical agents do not positively affect the physico-chemical properties of materials and improve their adsorption capacities [22]. For example, Luo et al. [60] revealed that lignin activation of a corn cob biochar decreased the adsorption capacity of Cd. Huang et al. [23], by modifying a rice husk biochar with iron oxide, decreased the adsorption capacity of Cd^{2+} from 58.65 to 42.48 mg/g. Similarly, Gao et al. [61] found that upon modifying a biochar using ammonium chloride as an activating agent, Cu adsorption capacity decreased.

Regarding the adsorption capacity based on the carboxylic, lactonic, and phenolic surface groups present in each material, significant differences were found in terms of type and the abundance in each biochar. Therefore, it is quite difficult to generalize trends related to different materials. For example, the phenolic surface groups present in the UBSB could influence the adsorption process; however, these functional groups are lower in the CAC, which generally showed the best results, whereas the material with the highest number of phenolic groups did not show the best results comparable with the CAC. Therefore, it is not possible to find a close relationship between the superficial functional groups and the removed contaminants based on current results. Additionally, most of the adsorbents presented phenolic groups, except for the BSBF-Na material. Thus, a normalization of the maximum adsorption capacity per mmol of phenolic groups was performed (Table 7); however, no difference was observed in the defined trend as the said value varies indistinctly from the material, the type, and abundance of the functional groups. Thus, in the present study, no direct correlation has been found between the adsorption of contaminants and the presence or abundance of distinct acid functional groups, since their behavior is similar to that of the other functional groups (lactonic and carboxylic).

However, when normalizing the maximum adsorption capacity of each material using the total amount of acid surface groups (Table 8), it was found that the materials with the highest adsorption capacity in $mg_{metal}/mmol_{total\ surface\ functional\ groups}$, for most metals, were CAC

Table 6
Adsorption capacity for each synthetized adsorbent in mg_{metal}/g_{ads}

Metal	Adsorption capacity × 10^{-2} (mg_{metal}/g_{ads})					
	USB	UBSB	BSBF-Na	BSBF-Zn	BSBF-Fe	CAC
Cr	0.4	1.8	0.0	0.0	0.8	1.8
Fe	0.4	130.9	51.2	3.9	61.6	115.5
Ni	0.4	7.8	1.9	0.0	10.2	80.6
Zn	3.0	35.7	0.0	0.0	20.4	214.2
Cu	15.4	61.6	66.0	15.4	35.2	84.7

Table 7
Normalization of adsorption capacity for each synthetized adsorbent in $mg_{metal}/mmol_{phenolic\ groups}$

Metal	Adsorption capacity ($mg_{metal}/mmol_{phenolic\ groups}$)					
	USB	UBSB	BSBF-Na	BSBF-Zn	BSBF-Fe	CAC
Cr	0.58	11.83	0.07	5.75	2.25	2.80
Fe	0.59	850.00	913.39	770.00	162.96	177.69
Ni	0.68	50.91	34.29	0.00	27.09	124.06
Zn	4.53	231.82	0.00	0.00	53.97	329.54
Cu	23.46	400.00	1,178.57	3,080.00	93.12	130.31

Table 8
Normalization of adsorption capacity for each synthetized adsorbent in $mg_{metal}/mmol_{total\ surface\ functional\ groups}$

Metal	Adsorption capacity ($mg_{metal}/mmol_{total\ surface\ functional\ groups}$)					
	USB	UBSB	BSBF-Na	BSBF-Zn	BSBF-Fe	CAC
Cr	0.34	0.14	–	0.01	0.35	4.97
Fe	0.35	10.06	–	0.90	25.68	315.32
Ni	0.40	0.60	–	0.00	4.27	220.15
Zn	2.67	2.74	–	0.00	8.50	584.77
Cu	13.81	4.73	–	3.62	14.67	231.23

and BSBF-Fe. These results clearly show that, on certain occasions, in adsorption processes, the total number of functional groups may be more relevant than the type of group present in the material.

The normalization of the adsorption capacity per m^2 of each material (Table 9) makes it possible to determine the adsorption capacity of each material based on its specific surface area, and to identify if this parameter is predominant in the present study or if there are other determining factors in adsorption processes. In relation to this parameter, it is observed that the UBSB and CAC materials present values close to each other, and even the UBSB yields higher values than the CAC in the adsorption of most contaminants despite having less surface area. This is interesting since it shows that the adsorption processes in the materials obtained in the present study do not show a direct relationship with the increase or decrease of the specific surface area. Regarding the other materials (USB, BSBF-Na, BSBF-Zn, BSBF-Fe), no specific trend is observed. Liu et al. [62] produced a biochar from walnut shells through pyrolysis at 550°C, using H_3PO_4 as a chemical modifier. They found that the average pore size decreased from 2.67 to 2.43 nm. According to the researchers, such changes in porosity were caused by specific interactions between the acids and the amorphous cellulose. The degradation of the amorphous cellulose caused the pores to collapse. Hafeez et al. [63] observed a similar phenomenon. Modification of biochar using inorganic acids was found to cause a deterioration in its textural properties [62].

On the other hand, Table 10 shows that, while performing the normalization of the adsorption capacity based on the pore volume of the adsorbent (mg contaminant/vol pore adsorbent), the highest amount of adsorbed contaminant was obtained using the UBSB material. This shows that this material, despite having a smaller pore volume than the CAC, can retain a greater amount of the various evaluated pollutants.

Again, regarding the pore size of the materials and its relationship with adsorption results, it is evident that the biochars with the best adsorption results (CAC and UBSB) have the highest pore diameters (41.1 and 33.8 nm, respectively) in relation to the other materials (3.1–5.4 nm). Similarly, with respect to pore volume, the materials that showed the lowest performance in terms of adsorption capacity and % removal (USB and BSBF-Zn) also showed the smallest pore volumes (0.0055 and 0.00045 cm^3/g, respectively). Initially, it might be assumed that, since the diameters of the hydrated ions [0.6 nm for Cu(II), Zn(II), Ni(II), Fe(II) and 0.9 nm for Cr(III)] are significantly smaller than the pore diameters, these might not constitute a determining factor. However, the results suggest that it is possible to find a relationship between the diameter and the pore volume and the adsorption capacity, wherein the material that shows the best CAC results also has the largest diameter and pore volume. Thus, while diameter and pore volume may not be the only factors that affect the adsorption process, they do seem to have a great effect, according to the present study.

The normalization of adsorption capacity with respect to various parameters clearly shows that the maximum adsorption capacity of various materials is complex and does not depend on a single parameter. Apparently, it is not always necessary to carry out a chemical modification of the biochar to achieve high adsorption capacities. For instance, an unfunctionalized biochar had a significantly high adsorption capacity with respect to the other synthesized materials and was comparable to CAC. By comparing the UBSB and CAC materials in terms of pore volume (0.0198 vs. 0.94 cm^3/g, respectively) and their general adsorption capacities, it can be assumed that procuring a material of lignocellulosic origin with greater pore volume could overcome the CAC challenges.

Finally, regarding the adsorption mechanisms for the removal of various metals, given the differences and complexity in the surface composition of each adsorbent and the various interactions that can occur between the adsorbate and the adsorbent, it is not possible to fully elucidate the mechanisms of these adsorption processes. In the literature, various phenomena or mechanisms have been proposed to explain how adsorbent heavy metals of a nature similar to those synthesized in the present work behave: electrostatic interaction (attraction or repulsion), ionic exchange, surface precipitation, and physical adsorption [18,22]. This depends both on the surface composition of the material and on the chemical nature of the adsorbate. Knowledge of the isoelectric point and the type and concentration of functional groups present in the material is key to elucidating the most predominant mechanisms in the adsorption process. Regarding the value corresponding to the isoelectric point, it can be observed that it oscillates between 6.4 and 7.4 in all materials (Table 4); these values are very close to neutral pH, which is consistent with the literature [56]. Accordingly, it would be expected that, at pH values of the wastewater below the isoelectric point, the adsorption of anionic species would be favored, since the surface of the

Table 9
Normalization of adsorption capacity for each synthetized adsorbent in mg_{metal}/m^2

	Adsorption capacity (mg_{metal}/m^2)					
Metal	USB	UBSB	BSBF-Na	BSBF-Zn	BSBF-Fe	CAC
Cr	1.67	0.12	0.00	0.06	0.02	0.03
Fe	1.67	8.50	9.13	7.70	1.63	1.78
Ni	1.95	0.51	0.34	0.00	0.27	1.24
Zn	12.93	2.32	0.00	0.00	0.54	3.30
Cu	66.96	4.00	11.79	30.80	0.93	1.30

Table 10
Normalization of adsorption capacity for each synthetized adsorbent in mg_{metal}/cm^3 pore

Metal	Adsorption capacity (mg_{metal}/cm^3 pore)					
	USB	UBSB	BSBF-Na	BSBF-Zn	BSBF-Fe	CAC
Cr	0.70	0.92	0.00	0.64	0.03	0.02
Fe	0.70	66.11	8.12	85.56	2.12	1.23
Ni	0.81	3.96	0.30	0.00	0.35	0.86
Zn	5.41	18.03	0.00	0.00	0.70	2.28
Cu	28.00	31.11	10.48	342.22	1.21	0.90

materials would be positively charged. However, the speciation diagrams obtained for the metals analyzed show that they are found predominantly in their lowest valence cationic form (Fe^{2+}, Cu^{2+}, Ni^{2+}, Cr^{3+} and Zn^{2+}). Thus, according to the pH value of the wastewater (3.65), it may be expected that there would be a process of electrostatic repulsion. This suggests that other phenomena prevail regarding the removal of metals using the materials evaluated in the present study.

Although very encouraging results were achieved in this research, other problems and challenges inevitably will come out. The first issue is related to adsorbent regeneration. How to effectively desorb the pollutants adsorbed on the biochar for subsequent safe treatment and the recycling of the adsorbed metals are well are the issues that need to be considered since the regeneration could enhance the economic and environmental sustainability of adsorption processes. The second is the issue of environmental risks. The stability and environmental risk of saturated biochar with pollutants have become the focus of current research. The third is the improvement of textural and morphological characteristics of the biochars. The fourth is on the adsorption mechanism of biochar using real wastewater. How the pollutants are absorbed in biochar still needs more in-depth research. Many existing studies have explained this because of several interacting mechanisms. However, it is still unclear which mechanism plays a leading role and how much it contributes. Clarifying these issues is of great significance for improving the adsorption capacity and environmental applications of the adsorbents. At the same time, the solution to these problems is also the key to future industrialization applications. Future research should focus on solving these problems mentioned above. In summary, the research and development prospects of unmodified biochar in the treatment of real wastewater are promising.

4. Conclusions

The results of the maximum adsorption capacities for each metal using each synthesized material show that a type of adsorbent under certain adsorption conditions can have a high capacity for the simultaneous removal of one or more heavy metals, while for others it might not. Therefore, in this study, it is not possible to affirm that there is an ideal adsorbent for the complete removal of all heavy metals found in the real wastewater analyzed. This demonstrates the importance of evaluating the effectiveness of an adsorbent by using real effluents, in order to elucidate various phenomena of competition and inhibition among contaminants in active sites.

The maximum adsorption capacities for most of the metals were obtained by using the adsorbent without any chemical agent. In addition, the values obtained for this material are comparable with those of CAC. This is interesting, since it is not necessary to carry out additional processes of chemical activation that imply energy expenditure, use of reagents, and waste generation. Also, it is replacing CAC with materials derived from agro-industrial waste is an attractive option. However, such research must continue to be carried out, not only with wastewater from the electroplating sector but also with effluents from other productive sectors. This would provide technical and economic bases for the application of these adsorbents in the decontamination of effluents and simultaneous minimization of the environmental impacts of the manufacturing sector. Additionally, it is difficult to compare the results of this study with other investigations since there are very few explorations regarding the adsorption processes for such real effluents. Further, it is not possible to radically affirm that the adsorbents obtained are ideal for removing heavy metals present in any wastewater generated from the electroplating sector, with the same efficiency. This is because manufacturing processes change over time and hence the physico-chemical characteristics of the RRW become random. However, the results of this study show that it is possible to use cheap adsorbents for the efficient and simultaneous removal of heavy metals, without the involvement of expensive, polluting, and complex chemical processes.

The environmental significance of this research is supported by the high adsorption capacities shown by the unfunctionalized adsorbent obtained from agricultural waste for the removal of high concentration levels of different toxic heavy metals present in real wastewater, this is a novel proposal because most studies using synthetic wastewater in which one or few metal types are present. However, the achieved conditions for the optimal removal of contaminant removal in laboratory experiments can be often difficult to control and maintain in real field conditions. Therefore, future studies should also focus on the pilot-scale process. Additionally, for future investigations, including more attention to impacts of operational and environmental factors, more economical calculations as well as isotherm studies on the prepared materials. The best techniques to achieve efficient metals recovery with less environmental impact and low cost are still under development and should be considered in future research. Furthermore, disposal of such adsorbents after the adsorption process is a big challenge to avoid environmental risks.

Acknowledgments

Authors are grateful for the financial support from the Politécnico Colombiano Jaime Isaza Cadavid, Colombia for the research titled "Construcción y evaluación de un filtro de biochar de banano para la remoción de metales pesados presentes en aguas residuales no domésticas", Research Group on Environmental Catalysis and Renewable Energies (CAMER).

Declaration of competing interest

The authors declare that they have no known competing financial interests or personal relationships that could have appeared to influence the work reported in this paper.

References

[1] H. Liu, S. Ning, S. Zhang, X. Wang, L. Chen, T. Fujita, Y. Wei, Preparation of a mesoporous ion-exchange resin for efficient separation of palladium from simulated electroplating wastewater, J. Environ. Chem. Eng., 10 (2022) 106966, doi: 10.1016/j.jece.2021.106966.

[2] X. Yang, Y. Wang, H. Ben, J. Yang, W. Jiang, A. Holmen, Y. Huang, D. Chen, Dynamics of Co/Co_2C redox cycle and their catalytic consequences in Fischer–Tropsch synthesis on cobalt–manganese catalysts, Chem. Eng. J., 455 (2023) 140577, doi: 10.1016/j.cej.2022.140577.
[3] A. Ghorpade, M.M. Ahammed, Water treatment sludge for removal of heavy metals from electroplating wastewater, Environ. Eng. Res., 23 (2018) 92–98.
[4] S.S. Moersidik, R. Nugroho, M. Handayani, Kamilawati, M.A. Pratama, Optimization and reaction kinetics on the removal of nickel and COD from wastewater from electroplating industry using electrocoagulation and advanced oxidation processes, Heliyon, 6 (2020) e03319, doi: 10.1016/j.heliyon.2020.e03319.
[5] G. Pooja, P.S. Kumar, G. Prasannamedha, S. Varjani, D.V.N. Vo, Sustainable approach on removal of toxic metals from electroplating industrial wastewater using dissolved air flotation, J. Environ. Manage., 295 (2021) 113147, doi: 10.1016/j.jenvman.2021.113147.
[6] J. Qu, X. Tian, Z. Jiang, B. Cao, M.S. Akindolie, Q. Hu, C. Feng, Y. Feng, X. Meng, Y. Zhang, Multi-component adsorption of Pb(II), Cd(II) and Ni(II) onto microwave-functionalized cellulose: kinetics, isotherms, thermodynamics, mechanisms and application for electroplating wastewater purification, J. Hazard. Mater., 387 (2020) 121718, doi: 10.1016/j.jhazmat.2019.121718.
[7] Y. Huo, A. Khan, Y. Liu, Z. Wang, Y. Yu, T. Sun, D. Liang, T. Su, K. Ri, X. Xie, S. Zhu, Z. Wang, Conversion of Fe-bearing minerals in sludge to nanorod erdite for real electroplating wastewater treatment: comparative study between ferrihydrite, hematite, magnetite, and troilite, J. Cleaner Prod., 298 (2021) 126826, doi: 10.1016/j.jclepro.2021.126826.
[8] M. Li, Y. Hu, N. Zhou, S. Wang, F. Sun, Hydrothermal treatment coupled with pyrolysis and calcination for stabilization of electroplating sludge: speciation transformation and environmental risk of heavy metals, J. Hazard. Mater., 438 (2022) 129539, doi: 10.1016/j.jhazmat.2022.129539.
[9] G. Peng, S. Deng, F. Liu, T. Li, G. Yu, Superhigh adsorption of nickel from electroplating wastewater by raw and calcined electroplating sludge waste, J. Cleaner Prod., 246 (2020) 118948, doi: 10.1016/j.jclepro.2019.118948.
[10] M.F. Mubarak, A.M. Zayed, H.A. Ahmed, Activated carbon/carborundum@microcrystalline cellulose core shell nanocomposite: synthesis, characterization and application for heavy metals adsorption from aqueous solutions, Ind. Crops Prod., 182 (2022) 114896, doi: 10.1016/j.indcrop.2022.114896.
[11] S.B. Betancur, S.A. Gil, A.N. Ardila A., A.V. Erasmo, B.Z. Rolando, J.A. Hernández, T.A. Zepeda, Developing bioadsorbents from orange peel waste for treatment of raw textile industry wastewater, Desal. Water Treat., 250 (2022) 80–99.
[12] Nilamsari, Sofyana, M.R. Lubis, D. Prilyanti, T. Maimun, Combination of adsorption process using bioadsorbent from coffee ground and ultrafiltration membrane in removing iron and lead content from water, Mater. Today Proc., 63 (2022) S115–S121.
[13] S. Kokate, K. Parasuraman, H. Prakash, Adsorptive removal of lead ion from water using banana stem scutcher generated in fiber extraction process, Results Eng., 14 (2022) 100439, doi: 10.1016/j.rineng.2022.100439.
[14] N. Ayala-Ruíz, D.H. Malagón-Romero, H.A. Milquez-Sanabria, Exergoeconomic evaluation of a banana waste pyrolysis plant for biofuel production, J. Cleaner Prod., 359 (2022) 132108, doi: 10.1016/j.jclepro.2022.132108.
[15] Q. Wang, C. Zhou, Y.-j. Kuang, Z.-h. Jiang, M. Yang, Removal of hexavalent chromium in aquatic solutions by pomelo peel, Water Sci. Eng., 13 (2020) 65–73.
[16] H. Yu, L. Zheng, T. Zhang, J. Ren, W. Cheng, L. Zhang, P. Meng, Adsorption behavior of Cd(II) on TEMPO-oxidized cellulose in inorganic/organic complex systems, Environ. Res., 195 (2021) 110848, doi: 10.1016/j.envres.2021.110848.
[17] A. Gul, A. Ma'amor, N.G. Khaligh, N. Muhd Julkapli, Recent advancements in the applications of activated carbon for the heavy metals and dyes removal, Chem. Eng. Res. Des., 186 (2022) 276–299.
[18] A. Tomczyk, B. Kondracki, K. Szewczuk-Karpisz, Chemical modification of biochars as a method to improve its surface properties and efficiency in removing xenobiotics from aqueous media, Chemosphere, 312 (2023) 137238, doi: 10.1016/j.chemosphere.2022.137238.
[19] J.-y. Huang, J.-s. Liao, J.-r. Qi, W.-x. Jiang, X.-q. Yang, Structural and physico-chemical properties of pectin-rich dietary fiber prepared from citrus peel, Food Hydrocolloids, 110 (2021) 106140, doi: 10.1016/j.foodhyd.2020.106140.
[20] Z. Wu, Z. Chen, J. Tang, Z. Zhou, L. Chen, Y. Fang, X. Hu, J. Lv, Efficient adsorption and reduction of Cr(VI) in water using one-step H_3PO_4-assisted prepared Leersia Hexandra Swartz hydrochar, Mater. Today Sustainability, 21 (2023) 100260, doi: 10.1016/j.mtsust.2022.100260.
[21] M. Yin, X. Bai, D. Wu, F. Li, K. Jiang, N. Ma, Z. Chen, X. Zhang, L. Fang, Sulfur-functional group tunning on biochar through sodium thiosulfate modified molten salt process for efficient heavy metal adsorption, Chem. Eng. J., 433 (2022) 134441, doi: 10.1016/j.cej.2021.134441.
[22] A. Pathy, P. Pokharel, X. Chen, P. Balasubramanian, S.X. Chang, Activation methods increase biochar's potential for heavy-metal adsorption and environmental remediation: a global meta-analysis, Sci. Total Environ., 865 (2023) 161252, doi: 10.1016/j.scitotenv.2022.161252.
[23] F. Huang, S.M. Zhang, R.R. Wu, L. Zhang, P. Wang, R.B. Xiao, Magnetic biochars have lower adsorption but higher separation effectiveness for Cd^{2+} from aqueous solution compared to nonmagnetic biochars, Environ. Pollut., 275 (2021) 116485, doi: 10.1016/j.envpol.2021.116485.
[24] B. Gupta, A. Mishra, R. Singh, I.S. Thakur, Fabrication of calcite based biocomposites for catalytic removal of heavy metals from electroplating industrial effluent, Environ. Technol. Innovation, 21 (2021) 101278, doi: 10.1016/j.eti.2020.101278.
[25] Y. Zhou, Z. Liu, A. Bo, T. Tana, X. Liu, F. Zhao, S. Sarina, M. Jia, C. Yang, Y. Gu, H. Zheng, H. Zhu, Simultaneous removal of cationic and anionic heavy metal contaminants from electroplating effluent by hydrotalcite adsorbent with disulfide (S^{2-}) intercalation, J. Hazard. Mater., 382 (2020) 121111, doi: 10.1016/j.jhazmat.2019.121111.
[26] T. Karuppiah, U. Uthirakrishnan, S.V. Sivakumar, S. Authilingam, J. Arun, R. Sivaramakrishnan, A. Pugazhendhi, Processing of electroplating industry wastewater through dual chambered microbial fuel cells (MFC) for simultaneous treatment of wastewater and green fuel production, Int. J. Hydrogen Energy, 47 (2022) 37569–37576.
[27] A.T. Vo, V.P. Nguyen, A. Ouakouak, A. Nieva, B.T. Doma, H.N. Tran, H.-P. Chao, Efficient removal of Cr(VI) from water by biochar and activated carbon prepared through hydrothermal carbonization and pyrolysis: adsorption-coupled reduction mechanism, Water, 11 (2019) 1164, doi: 10.3390/w11061164.
[28] H. Ma, J. Yang, X. Gao, Z. Liu, X. Liu, Z. Xu, Removal of chromium(VI) from water by porous carbon derived from corn straw: influencing factors, regeneration and mechanism, J. Hazard. Mater., 369 (2019) 550–560.
[29] A. Kumar, H.M. Jena, Adsorption of Cr(VI) from aqueous phase by high surface area activated carbon prepared by chemical activation with $ZnCl_2$, Process Saf. Environ. Prot., 109 (2017) 63–71.
[30] I. Enniya, L. Rghioui, A. Jourani, Adsorption of hexavalent chromium in aqueous solution on activated carbon prepared from apple peels, Sustainable Chem. Pharm., 7 (2018) 9–16.
[31] A.S.K. Kumar, S.-J. Jiang, W.-L. Tseng, Effective adsorption of chromium(VI)/Cr(III) from aqueous solution using ionic liquid functionalized mulitwalled carbon nanotube as a super sorbent, J. Mater. Chem. A, 3 (2015) 7044–7057.
[32] N.K. Hamadi, X. Dong, M.M. Farid, M.G.Q. Lu, Adsorption kinetics for the removal of chromium(VI) from aqueous solution by adsorbents derived from used tyres and sawdust, Chem. Eng. J., 84 (2001) 95–105.

[33] H. Kim, R.A. Ko, S. Lee, K. Chon, Removal efficiencies of manganese and iron using pristine and phosphoric acid pre-treated biochars made from banana peels, Water (Switzerland), 12 (2020) 1–13.
[34] P.F. Santos, J.B. Neris, F.H.M. Luzardo, F.G. Velasco, M.S. Tokumoto, R.S. da Cruz, Chemical modification of four lignocellulosic materials to improve the Pb^{2+} and Ni^{2+} ions adsorption in aqueous solutions, J. Environ. Chem. Eng., 7 (2019) 103363, doi: 10.1016/j.jece.2019.103363.
[35] A.A. Oladipo, E.O. Ahaka, M. Gazi, High adsorptive potential of calcined magnetic biochar derived from banana peels for Cu^{2+}, Hg^{2+}, and Zn^{2+} ions removal in single and ternary systems, Environ. Sci. Pollut. Res., 26 (2019) 31887–31899.
[36] R. Foroutan, S.J. Peighambardoust, R. Mohammadi, S.H. Peighambardoust, B. Ramavandi, Cadmium ion removal from aqueous media using banana peel biochar/Fe_3O_4/ZIF-67, Environ. Res., 211 (2022) 113020, doi: 10.1016/j.envres.2022.113020.
[37] Y. Sun, J. Chen, Z. Wei, Y. Chen, C. Shao, J. Zhou, Aspects copper ion removal from aqueous media using banana peel biochar/Fe_3O_4/branched polyethyleneimine, Colloids Surf., A, 658 (2023) 130736, doi: 10.1016/j.colsurfa.2022.130736.
[38] N. Zhou, H. Chen, J. Xi, D. Yao, Z. Zhou, Y. Tian, X. Lu, Biochars with excellent Pb(II) adsorption property produced from fresh and dehydrated banana peels via hydrothermal carbonization, Bioresour. Technol., 232 (2017) 204–210.
[39] Z. Ahmad, B. Gao, A. Mosa, H. Yu, X. Yin, A. Bashir, H. Ghoveisi, S. Wang, Removal of Cu(II), Cd(II) and Pb(II) ions from aqueous solutions by biochars derived from potassium-rich biomass, J. Cleaner Prod., 180 (2018) 437–449.
[40] A.F. Torres Puentes, Evaluación de parámetros en la filtración rápida como tratamiento de agua gris doméstica, Universidad de Los Andes Facultad, 2017.
[41] A.M. Kennedy, M. Arias-Paic, Fixed-bed adsorption comparisons of bone char and activated alumina for the removal of fluoride from drinking water, J. Environ. Eng., 146 (2020) 04019099, doi: 10.1061/(asce)ee.1943-7870.0001625.
[42] S. Rajoria, M. Vashishtha, V.K. Sangal, Review on the treatment of electroplating industry wastewater by electrochemical methods, Mater. Today Proc., 47 (2021) 1472–1479.
[43] M. de A. y D. Sostenible, Resolución 0631 del 17 de marzo de 2015, Por La Cual Se Establ. Los Parámetros y Los Valores Límites Máximos Permis. En Los Vertimientos Puntuales a Cuerpos Agua Supeficiales y a Los Sist. Alcantarilladopúblico y Se Dictan Otras Disposiciones, 2015, pp. 1–62.
[44] M.T. Amin, A.A. Alazba, M. Shafiq, Removal of copper and lead using banana biochar in batch adsorption systems: isotherms and kinetic studies, Arabian J. Sci. Eng., 43 (2018) 5711–5722.
[45] G.A. Adebisi, Z.Z. Chowdhury, S.B.A. Hamid, E. Ali, Hydrothermally treated banana empty fruit bunch fiber activated carbon for Pb(II) and Zn(II) removal, BioResources, 11 (2016) 9686–9709.
[46] M. Waqas, A. Aburizaiza, R. Miandad, M. Rehan, M. Barakat, D.A.-S. Nizami, Development of biochar as fuel and catalyst in energy recovery technologies, J. Cleaner Prod., 188 (2018) 477–488.
[47] S. Khoshk, A. Tahmasebi, R. Wang, J. Dou, J. Yu, Formation mechanism of nano graphitic structures during microwave catalytic graphitization of activated carbon, Diamond Relat. Mater., 120 (2021) 108699, doi: 10.1016/j.diamond.2021.108699.
[48] M.F. Aly Aboud, Z.A. Alothman, M.A. Habila, C. Zlotea, M. Latroche, F. Cuevas, Hydrogen storage in pristine and d10-block metal-anchored activated carbon made from local wastes, Energies, 8 (2015) 3578–3590.
[49] E.I. Inam, U.J. Etim, E.G. Akpabio, S.A. Umoren, Simultaneous adsorption of lead(II) and 3,7-bis(dimethylamino)-phenothiazin-5-ium chloride from aqueous solution by activated carbon prepared from plantain peels, Desal. Water Treat., 57 (2016) 6540–6553.
[50] P. Dutournié, M. Bruneau, J. Brendlé, L. Limousy, S. Pluchon, Mass transfer modelling in clay-based material: estimation of apparent diffusivity of a molecule of interest, C.R. Chim., 22 (2019) 250–257.
[51] C. Sun, T. Chen, Q. Huang, M. Zhan, X. Li, J. Yan, Activation of persulfate by CO_2-activated biochar for improved phenolic pollutant degradation: performance and mechanism, Chem. Eng. J., 380 (2020) 122519, doi: 10.1016/j.cej.2019.122519.
[52] M. Patel, R. Kumar, C.U. Pittman, D. Mohan, Ciprofloxacin and acetaminophen sorption onto banana peel biochars: environmental and process parameter influences, Environ. Res., 201 (2021) 111218, doi: 10.1016/j.envres.2021.111218.
[53] M.M. Rahman, A.Z. Shafiullah, A. Pal, M.A. Islam, I. Jahan, B.B. Saha, Study on optimum IUPAC adsorption isotherm models employing sensitivity of parameters for rigorous adsorption system performance evaluation, Energies, 14 (2021), doi: 10.3390/en14227478.
[54] D.C.O. Valencia, M. del R.S. Kou, Estudio comparativo de la capacidad de adsorción de Cadmio utilizando carbones activados preparados a partir de semillas de aguaje y de aceituna, Universidad Católica de Perú, 2015. Available at: https://doi.org/10.13140/RG.2.1.2075.6322
[55] J.G.D. Nemaleu, R.C. Kaze, S. Tome, T. Alomayri, H. Assaedi, E. Kamseu, U.C. Melo, V.M. Sglavo, Powdered banana peel in calcined halloysite replacement on the setting times and engineering properties on the geopolymer binders, Constr. Build. Mater., 279 (2021) 122480, doi: 10.1016/j.conbuildmat.2021.122480.
[56] M. Qiu, L. Liu, Q. Ling, Y. Cai, S. Yu, S. Wang, D. Fu, B. Hu, X. Wang, Biochar for the removal of contaminants from soil and water: a review, Biochar, 4 (2022) 1–25.
[57] R.T. Kapoor, M. Rafatullah, M.R. Siddiqui, M.A. Khan, M. Sillanpää, Removal of Reactive Black 5 dye by banana peel biochar and evaluation of its phytotoxicity on tomato, Sustainability, 14 (2022) 4176, doi: 10.3390/su14074176.
[58] J. Cui, X. Wang, Y. Yuan, X. Guo, X. Gu, L. Jian, Combined ozone oxidation and biological aerated filter processes for treatment of cyanide containing electroplating wastewater, Chem. Eng. J., 241 (2014) 184–189.
[59] Z. Ma, Z. Cheng, Y. Yang, C. Nie, D. Wu, T. Yang, S. Wang, D. Li, Acid-modified anaerobic biogas residue biochar activates persulfate for phenol degradation: enhancement of the efficiency and non-radical pathway, Colloids Surf., A, 663 (2023) 131121, doi: 10.1016/j.colsurfa.2023.131121.
[60] M. Luo, H. Lin, B. Li, Y. Dong, Y. He, L. Wang, A novel modification of lignin on corncob-based biochar to enhance removal of cadmium from water, Bioresour. Technol., 259 (2018) 312–318.
[61] Y. Gao, X. Zhu, Q. Yue, B. Gao, Facile one-step synthesis of functionalized biochar from sustainable prolifera-green-tide source for enhanced adsorption of copper ions, J. Environ. Sci. (China), 73 (2018) 185–194.
[62] C. Liu, W. Wang, R. Wu, Y. Liu, X. Lin, H. Kan, Y. Zheng, Preparation of acid- and alkali-modified biochar for removal of methylene blue pigment, ACS Omega, 5 (2020) 30906–30922.
[63] A. Hafeez, T. Pan, J. Tian, K. Cai, Modified biochars and their effects on soil quality: a review, Environments, 9 (2022) 60, doi: 10.3390/environments9050060.